Atomic and electronic structure of crystalline and amorphous alloys. II. Strong electronic bonding effects in Ca-Al compounds

J. Hafner and S. S. Jaswal*
Institut für Theoretische Physik, Technische Universität Wien, Karlsplatz 13, A-1040 Wien, Austria
(Received 9 October 1987; revised manuscript received 13 April 1988)

Calculations of the atomic and electronic structure of Ca_xAl_{1-x} glasses (with $x=0.70$, 0.60, 0.50, and 0.33) and of the crystalline intermetallic compound $CaAl_2$ are presented. For the amorphous alloys the calculations are based on realistic models for the atomic structure constructed by a molecular-dynamics simulation linked to a steepest-descent potential-energy mapping. The effective interatomic forces are calculated using pseudopotential theory. We find that both the atomic and the electronic structures are dominated by strong electronic bonding effects: (a) The strong (s,p,d) hybridization of the free-electron-like conduction band of pure Al is broken up on alloying with Ca, and we find nearly separate Al $3s$ and Al $3p$ bands which are much narrower than the s and p bands in pure Al; (b) only the Al $3p$ states interact substantially with the Ca states. The interatomic electron transfer is small, but we find a substantial intra-atomic d-to-s transfer on the Al sites and an s-to-d transfer on the Ca sites. In the atomic structure the s-d promotion leads to a strong contraction of the Ca-Ca bonds in both the crystalline and the amorphous alloys compared to pure Ca, and a preferential Ca-Al bonding in the Al-rich but not in the Ca-rich alloys. The calculated electronic structure is well confirmed in all its details by heat-capacity, photoemission, and soft-x-ray emission spectra. The x-ray-diffraction data for the atomic structure corroborate the predicted compression of the Ca-Ca distances and the overall form of the correlation functions (which points to a local topology best described as a disordered tetrahedral close packing) but show distinctly lower and broader peaks. We argue that this is due to the short mean free path of the electrons, which will lead to a damping of the oscillations in the interatomic interactions.

I. INTRODUCTION

Recently, considerable attention has been devoted to the interesting contrast in the properties of Ca_xMg_{1-x} and Ca_xAl_{1-x} glasses. For example, a Ca_7Mg_3 glass has a low resistivity ($\rho\sim 45$ $\mu\Omega$ cm), a positive temperature coefficient of resistivity (TCR), and a large and positive thermopower ($S\sim 7$ μV/K),[1-3] whereas Ca_xAl_{1-x} glasses have high resistivities (increasing from $\rho\sim 170$ $\mu\Omega$ cm at $x=0.8$ to 400 $\mu\Omega$ cm at $x=0.60$), a strongly negative TCR, and a considerably smaller thermopower ($S\sim 2$ μV/K).[4-7] The difference in the electronic transport properties has often been attributed to the population of Ca $3d$ states and an associated strong electron-ion-scattering potential in Ca-Al, but not in Ca-Mg, glasses.[6,7] However, measurements of the electronic specific heat show that the density of states at the Fermi level is strongly enhanced compared to the free-electron (FE) value in Ca-Mg glasses ($\gamma_{\rm expt}/\gamma_{\rm FE}=1.6$ for Ca_7Mg_3) and much less so in the Ca-Al glasses ($\gamma_{\rm expt}/\gamma_{\rm FE}=1.2$ for Ca_7Al_3).[3,8] Photoelectron spectroscopy suggests the existence of a minimum in the electronic density of states (DOS) at about 3 eV below the Fermi level and SXS (soft-x-ray spectroscopy) investigations show a narrowing of the Al $3p$ band in Ca-Al glasses compared to pure Al.[9] No similar effects are observed in Ca-Mg glasses.

There are also pronounced differences in the atomic structures. Ca-Mg glasses have very sharp peaks in both the reduced pair distribution function $G(R)$ and in the static structure factor $S(Q)$ observed by x-ray diffraction.[10] The peaks measured for Ca-Al are much lower, broader, and more asymmetric.[7,11] In both cases the Ca-Ca nearest-neighbor distances are substantially shorter than in pure Ca, but this compression is much more pronounced in Ca-Al than in Ca-Mg.

Very recently, we presented an *ab initio* calculation of the atomic and electronic structure of Ca-Mg glasses[12,13] (hereafter Ref. 13 will be referred to as paper I). The calculations are based on pseudopotential-derived interatomic forces, a molecular-dynamics simulation linked to a steepest-descent potential-energy mapping for the calculation of the atomic structure, and a linearized-muffin-tin-orbital (LMTO) supercell technique for the calculation of the electronic structure. We achieve good agreement with both the x-ray-diffraction data for the atomic structure and the photoemission experiments for the electronic structure. The characteristic enhancement of the DOS at the Fermi level stems from the onset of the Ca $3d$ DOS over an essentially free-electron-like DOS of the sp electrons. Thus, it is impossible to attribute the different physical properties of Ca-Mg and Ca-Al glasses to a substantial d character of the electronic DOS in Ca-Al, but not in Ca-Mg. Finally, we found a strong correlation between not only the atomic, but also the electronic, structures of the metallic glass Ca_7Mg_3 and of the tetrahedrally close-packed intermetallic compound $CaMg_2$ (with the crystal structure of a hexagonal $MgZn_2$-type Laves phase).

 ©1988 The American Physical Society

In the present paper we extend these investigations to Ca-Al alloys in the crystalline and amorphous states. Ca-Al alloys, in general, differ from Ca-Mg alloys by much stronger chemical-bonding effects: The heat of formation of the Laves-phase $CaAl_2$ is 4 times as large as that of the Laves-phase $CaMg_2$. Ca-Al glasses may be formed over a much larger composition range and have a higher thermal stability. It is remarkable that the very stable Laves-phase $CaAl_2$ is formed in spite of a rather unfavorable size factor: The ratio of the Goldschmidt radii is $R_{Ca}/R_{Al}=1.39$, whereas the ideal radius ratio for the formation of an AB_2 Laves phase is $R_A/R_B=1.225$.[14] Our previous calculations of the interatomic forces in Ca-based alloy[15,16] have shown that in Ca-Al the strong electronic bonding effects cause a pronounced variation of the interatomic potentials with concentration. Upon addition of Al, the effective diameter of the Ca atoms is compressed, and the strength of the Ca-Ca interactions is reduced. The Al-Al and Ca-Al potentials, on the other hand, become more attractive. The origin of both the "chemical compression" of the Ca atoms, and of the preferential Ca—Al bonding, have been discussed in relation to two competing charge-transfer effects arising from the electronegativity difference and the electroneutrality principle.[15–17]

Our present calculations of the self-consistent electronic structure for crystalline and glassy Ca-Al alloys confirm and extend this picture. As suggested by the pseudopotential calculations, the interatomic charge transfer is small. More important is an intra-atomic promotion from s to d on the Ca sites, and from d to s on the Al sites compared to the pure metals. This accounts for the observed variation of the effective atomic sizes. In addition, we find a strong dehybridization of the free-electron-like valence band of Al: With addition of Ca, the Al $3s$ states are lowered in energy relative to the Al $3p$ states; both the $3s$ and $3p$ bands are appreciably narrowed compared to pure Al. At the best glass-forming compositions there is only minimal overlap between the Al $3s$ and Al $3p$ bands. All the predictions of the electronic-structure calculations are well confirmed by photoemission, soft-x-ray, and heat-capacity measurements. It is interesting that the main difference between the Ca-Mg and Ca-Al glasses is not so much the difference in the d component of the DOS close to the Fermi level, but the different amount of s,p dehybridization: it is rather weak in the Ca-Mg and very strong in the Ca-Al glasses. Similar dehybridization effects are known to exist in "compound-forming" liquid alloys of alkali metals with polyvalent metals, which show strong ordering effects and high resistivities up to the onset of a metal-insulator transition.[18,19]

Our paper is organized as follows: In Sec. II we review briefly the chemical-bonding effects in the interatomic potentials and their relation to electron-transfer effects. In Sec. III we present the results for the atomic structures obtained with a molecular-dynamics simulation linked to a steepest-descent "potential-energy mapping," and the preparation of the "amorphous" supercells used in the calculation of the electronic structure with the linearized-muffin-tin-orbital method. The electronic structures calculated for the crystalline Laves-phase $CaAl_2$ and for glasses of the compositions $CaAl_2$, Ca_7Al_3, Ca_6Al_4, and Ca_5Al_5 are presented in Sec. IV (only for the Ca-rich alloys is a formation of a metallic glass by quenching from the melt is actually possible).

II. INTERATOMIC FORCES IN Ca-Al ALLOYS

Our method for calculating the interatomic forces in metals and alloys on the basis of pseudopotentials and linear-response theory is well documented elsewhere,[15,16] so we shall not repeat this here. In order to establish the connection between the electronic bonding effects manifested in the interatomic potentials and the electronic structure itself, it is important, however, to review very briefly the essential effects.

The basic physical arguments were anticipated by Pauling[20] long ago. He argued that the formation of the metallic bond in binary metallic systems is dominated by two competing charge-transfer effects. First, electrons are transferred in the direction expected from the electronegativity difference. This creates strong charge-density gradients which enhance the electron-electron potential energy. The alloy will try to reduce the potential energy by redistributing the electrons accordingly. This is Pauling's electroneutrality principle, which causes a second electron-transfer mechanism opposite to the first one.

Pauling's ideas are directly reflected in the pseudopotential formalism. Here we start from the homogeneous distribution of the free electrons into which the ions are introduced as a perturbation. Since the conduction-electron states must be orthogonal to the core states, a conduction electron acquires a high kinetic energy when entering the core region. Thus the probability of finding an electron in the core region is reduced. One says that each ion forms an "orthogonalization hole" in the Fermi sea. In the second step, electrons are allowed to flow to screen the ionic cores plus their orthogonalization holes. The core charge, the orthogonalization hole, and the screening charge together form the neutral pseudoatom in a metal.

In a binary alloy the electron-density distribution is given by a superposition of neutral A and B atoms, but chemical effects will result in a deformation of these pseudoatoms relative to their form in the pure metal. The ions with the lower valence (say, the A ions) will encounter an increased electron density in the alloy. Therefore they will have to form a larger orthogonalization hole, whereas that on the B ions will be smaller than in pure B metal. This is equivalent to a transfer of electrons from A to B, i.e., in the direction expected from the electronegativity difference. As the pseudoatoms as a whole are still electrically neutral, this will have to be compensated for by a redistribution of the screening charges. In an actual calculation one finds that not only is each pseudoatom neutral, but according to the electroneutrality principle the additional screening charge on the A ions accumulates in the core region.

The way in which the effective interatomic potentials follow the redistribution of the electronic charges is most

easily understood if we adopt a representation of the pair potentials due to Evans.[21] He showed that the interatomic interaction $\Phi_{ij}(R)$ can be written as the sum of an interaction between neutral pseudoatoms, $\Phi_{ij}^{n}(R)$, and a term related to the one-electron energy eigenvalues, $\Phi_{ij}^{1e}(R)$, i.e. (for convenience we adopt a Q-space representation),

$$\Phi_{ij}(Q)=\Phi_{ij}^{n}(Q)+\Phi_{ij}^{1e}(Q) , \tag{1}$$

with

$$\Phi_{ij}^{n}(Q)=8\pi\{Z_iZ_j-[1-G(Q)]\rho_i^{sc}(Q)\rho_j^{sc}(Q)\}/V_aQ^2 \tag{2}$$

and

$$\Phi_{ij}^{1e}(Q)=V_a\chi(Q)w_i^{sc}(Q)w_j^{sc}(Q) , \tag{3}$$

where $\rho_i^{sc}(Q)$ is the screening charge density, $w_i^{sc}(Q)$ the screened pseudopotential matrix element at atom i, $\chi(Q)$ the electron-gas susceptibility, and $G(Q)$ the local-field correction accounting for exchange and correlation effects in the electron gas. The neutral-pseudoatom interaction is repulsive at short distances, and has weak oscillations at large R. If the screening charges are more concentrated around the nucleus, the Coulomb repulsions will be screened over smaller distances—this accounts for the "chemical compression" of the electropositive atom A upon alloying with an electronegative atom B. Figures 1 and 2 illustrate this effect for two Ca-Al alloys. Note that the effective size of the Ca atom (measured in terms of the diameter of the repulsive core) is distinctly larger in the Ca-rich than in the Al-rich alloy. The one-electron part of the effective pair potential has pronounced Friedel oscillations, and it is affected by the change in the susceptibility and by the change of the pseudopotentials. The change in the susceptibility accounts for the largest effect. As a consequence of the change in the Fermi momentum k_F, the wavelength $\lambda_F=2\pi/2k_F$ of the Friedel oscillations will be smaller in the A-B alloy than in the pure metal A, but larger than in B. The changes in the interatomic interaction close to the nearest-neighbor distance result from the interplay of both effects, namely renormalization of the core size and shift of the Friedel oscillations. For the Al-Al interactions, for example, we find that with increasing Ca content of the alloy the diameter of the repulsive core of the Al atom is almost unchanged, whereas the Friedel oscillations are shifted to larger distances. This helps to expose the first attractive minimum in $\Phi_{\text{Al-Al}}(R)$, which is nearly

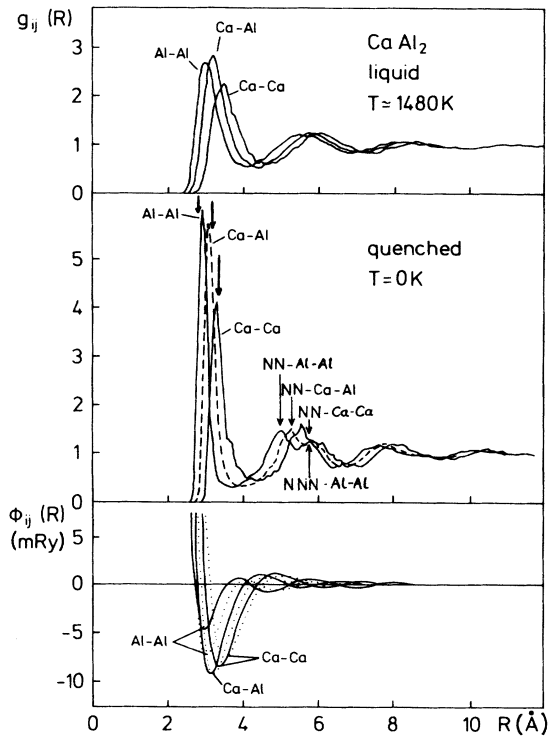

FIG. 1. Interatomic pair potentials $\Phi_{ij}(R)$ (solid curve, number density $n=0.046\,18$ Å^{-3}; dotted curves, $n=0.037\,19$ Å^{-3}) and pair-correlation functions $g_{ij}(R)$ for the liquid and for the glassy phases of $CaAl_2$. The vertical arrows indicate the first-, second-, and third-nearest-neighbor distances in the crystalline Laves-phase $CaAl_2$—note the coincidence with the peaks of the corresponding correlation function.

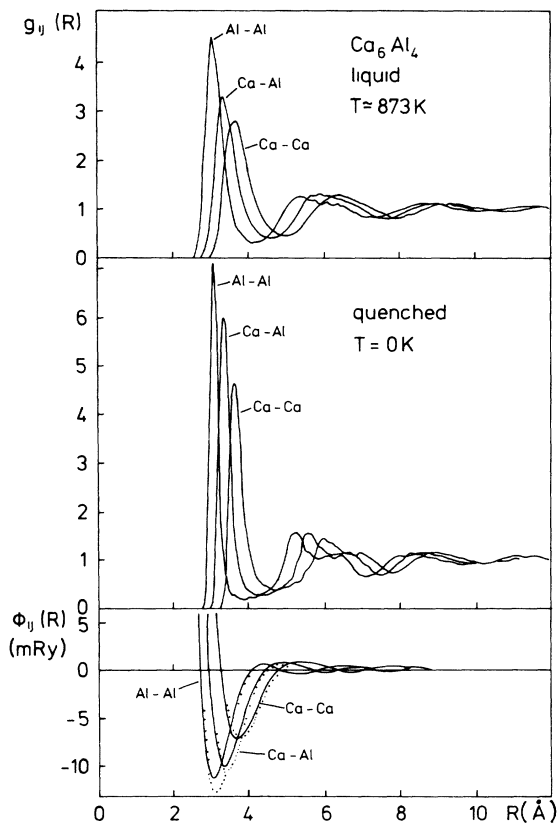

FIG. 2. Interatomic pair potentials $\Phi_{ij}(R)$ (solid curve, $n=0.033\,49$ Å^{-3}; dotted curve, $n=0.029\,75$ Å^{-3}) and pair-correlation functions $g_{ij}(R)$ for liquid and glassy Ca_6Al_4 alloys. See Fig. 1.

completely covered by the repulsive core in pure aluminum (see Hafner and Heine[22] for numerical and analytical studies of the variation of interatomic potentials with electron density and pseudopotential). A similar change is observed in the Ca-Al interaction. It leads to a very strong Ca-Al interaction in $CaAl_2$, promoting a pronounced tendency towards heterocoordination. The change in the Ca-Ca interactions is determined by the reverse effect: Upon adding Al the core size decreases, the Friedel oscillations are shifted inward, and the nearest-neighbor interaction is reduced. Note that the average nearest-neighbor distance at a fixed density is determined essentially by the position of the first attractive minimum in the pair potential. In the present case this means that the Al-Al distance is nearly independent of composition (both effects tend to compensate for each other), whereas the Ca-Ca distances are strongly reduced upon alloying with Al (both effects add up to give a rather considerable compression of the effective size of the Ca atoms).

The pseudopotentials are also affected by alloying. If the orthogonalization effect becomes stronger, the repulsive component of the pseudopotential is increased and the cancellation of the attractive electron-ion potential by the pseudopotential increases. On the other hand, a weaker orthogonalization effect is reflected in a stronger electron-ion interaction. Note that the more extended angular-momentum components of the conduction-band states will be less affected than those that are more localized close to the core region—this is a point to which we shall return when we discuss the electronic structure.

III. STRUCTURE MODELING

The greatest problem of static model-building algorithms for amorphous structures is their lack of sensitivity to the details of the interatomic forces. Very recently, Stillinger and Weber[23,24] have proposed a new simulation technique which overcomes this problem. The simulation starts with a molecular-dynamics calculation for the liquid phase, where thermodynamic equilibrium with respect to both the topological and chemical short-range order is easily achieved. Parallel to this equilibrium molecular-dynamics run, independent instantaneous configurations of the liquid are periodically mapped onto nearby minima in the potential energy. Stillinger and Weber have shown that the mapping results in a strong image enhancement of the local order in the liquid. Moreover, the correlation functions obtained by averaging over a sufficiently large number of mapped configurations are found to be independent of the thermodynamic parameters before the mapping. Hence they really represent the inherent structure of the liquid. It was suggested that this liquid-state inherent structure is an accurate model for the structure of the glass. We have taken up these suggestions and applied the molecular-dynamics simulation linked to a steepest-gradient potential-energy mapping to a number of simple-metal alloys.[11–13,25–27] Detailed comparisons with x-ray- and neutron-diffraction data and with extended x-ray-absorption fine-structure (EXAFS) experiments have demonstrated that the inherent structure of the liquid yields indeed to a quantitatively accurate description of the structure of metallic glasses. We refer to one of these papers[26] for details of the simulation technique. Here we extend these simulations to a number of Ca-Al glasses (first results for Ca_6Al_4, together with an energy-dispersive x-ray experiment have already been presented elsewhere[11]).

Figures 1 and 2 show the result of the molecular-dynamics simulations for liquid $CaAl_2$ and Ca_6Al_4 and the "quench" pair-correlation functions obtained by the potential-energy mapping. Again we find that the removal of the thermally induced distortions strongly enhances the image of the local order in the pair-correlation functions. We note in particular the following. (a) A strong compression of the Ca-Ca distances compared to the nearest-neighbor distance in face-centered-cubic Ca ($d=3.95$ Å), which increases with increasing Al content of the glass ($d_{\text{Ca-Ca}}=3.65$ Å in a-Ca_7Al_3 and $d_{\text{Ca-Ca}}=3.32$ Å in a-$CaAl_2$). This compression is also observed in the crystalline intermetallic compounds, e.g., in the cubic Laves-phase $CaAl_2$, we have $d_{\text{Ca-Ca}}=3.48$ Å. (b) A pronounced chemical short-range order in the Al-rich, but not in the Ca-rich, alloys. This is expected from the form of the interatomic potentials and again similar to the local order in the crystalline intermetallic compound: In $CaAl_2$ each Ca atom is surrounded by twelve Al and four Ca atoms, each Al atom by six Ca and six Al atoms. The similarity in the local order of the crystalline and of the quench-condensed phases extends even further. We find that the split second peak of the partial pair-correlation functions may be indexed in terms of second- and third-nearest-neighbor distances in the Laves phase. We can also analyze triplet correlation, most conveniently by considering the bond-angle distributions,[26,27] see Fig. 3. This shows that the local environments of the Ca and Al atoms are distinctly different. The distribution of the bond angles around the Al atoms has well defined peaks at the icosahedral bond

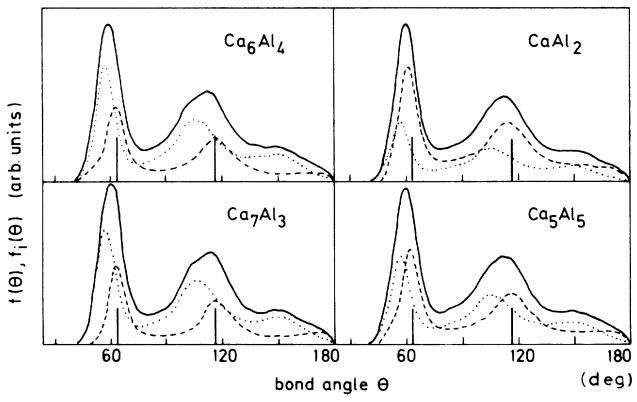

FIG. 3. Total bond-angle distribution function $f(\theta)$ (solid line) and partial bond-angle distribution functions $f_i(\theta)$ (dashed line, $i=$Al; dotted line, $i=$Ca) for amorphous Ca-Al alloys of different compositions. The vertical lines indicate the bond angles in a regular icosahedron.

angles ($\theta = 63.5°$, 116.5°, and 180°), suggesting that the Al atoms occupy sites with a predominantly icosahedral symmetry. The distribution of the bond angles around the Ca sites shows a different pattern: the two main peaks are shifted to smaller angles, a peak close to $\theta = 150°$ has appeared, and the number of near-collinear triplets is strongly reduced. As we have shown in earlier studies on Mg-Zn and Ca-Mg glasses,[13,26,27] this points to a local arrangement in the form of 14-, 15-, and 16-fold-coordinated Friauf polyhedra. Note that the Laves phases consist of interpenetrating icosahedra centered at the smaller atoms, and Friauf polyhedra with 16 vertices centered at the larger atoms.[14] Compared to Mg-Zn and Ca-Mg glasses, the differences in the partial bond-angle distributions are more pronounced in Ca-Al. Figure 3 also shows that the local symmetry does not change with composition. The local arrangements around the Ca atoms, in particular, seem to change very little, whereas the bond-angle distribution around the Al atoms becomes more diffuse in the Ca-rich range. It has been pointed out that the Friauf polyhedra may be derived from the regular icosahedron by the introduction of topological defects (disclination lines), with the Laves phases (and other closely related Frank-Kasper phases) forming a periodic array of disclination lines.[28,29] In the glassy phase this network is disturbed and entangled (the entanglement accounts for the resistance against crystallization). The difference between the quench-condensed phases in the compound- and glass-forming composition ranges is in the much larger number of topological defects in the latter.[26]

Of course, it is interesting to compare the predictions of the simulation studies with experiment. Up to now, only x-ray-diffraction experiments have been performed on Ca-Al glasses.[7,11] Figure 4 shows a typical result for a Ca_6Al_4 glass (for this composition both angle-dispersive and energy-dispersive diffraction experiments have been performed). We find that the predicted compression of the Ca-Ca nearest-neighbor distances from $d = 3.95$ Å in pure Ca to $d_{Ca\text{-}Ca} = 3.56$ Å in amorphous Ca_6Al_4 is fully confirmed by the experiment. On the other hand, we see that although the first peak in the calculated pair distribution function of Ca_6Al_4 is lower and broader than that of Ca_7Mg_3, the theory still underestimates the characteristic differences in the atomic structures of Ca-Al and Ca-Mg glasses. Preliminary results suggest that this is due to an electronic mean free path that is much shorter in Ca-Al than in Ca-Mg. A short mean free path of the electrons causes a smearing out of the logarithmic singularity in the electron-gas susceptibility and leads to a damping of the Friedel oscillations in the interatomic potentials. As the attractive minima of the interatomic potentials become shallower, the liquid or amorphous alloy orders less strongly, resulting in lower and broader peaks in the pair-correlation functions. However, since the mean free path depends on the atomic as well as the electronic structure, a complete answer would require a self-consistent calculation of both.

The molecular-dynamics and potential-energy–mapping calculations have been performed for samples of 800 atoms (for the remaining parameters, see paper I and Ref. 26) contained in a periodically repeated box with the shape of a rhombic dodecahedron. Such a large number of atoms is necessary for achieving a good statistical resolution for the calculated partial pair-correlation functions, but is much too large for performing supercell band-structure calculations. As in our work on Ca-Mg glasses (see paper I), we prepare smaller models containing about 60 atoms by cutting small cubes of appropriate size out of the 800-atom cells. The origin of the cubes is chosen such that they contain atoms of both species in the proper ratio and that, if the cube is periodically repeated, there are only minimal strains across its surfaces. The remaining strains are eliminated by a static relaxation.

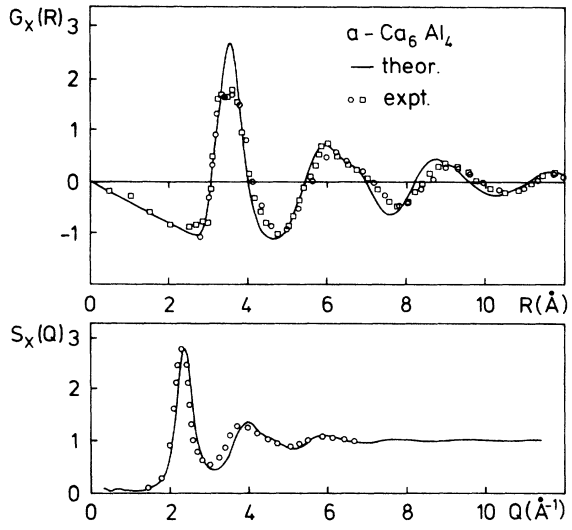

FIG. 4. X-ray-weighted reduced radial distribution function $G_x(R)$ and static structure factor $S_x(Q)$ for amorphous Ca_6Al_4 at room temperature. Solid line, calculated; open circles, energy-dispersive x-ray-diffraction results of Hafner *et al.* (Ref. 11); open squares, angle-dispersive x-ray-diffraction results of Naugle *et al.* (Ref. 7).

Figure 5 compares the partial pair-correlation functions calculated for a single 60-atom model with those obtained by taking an average over 20 mapped configurations of the 800-atom model. We find that even details of the correlation functions are reproduced with good accuracy, although the statistical fluctuations, as expected, are much larger in the smaller samples. The correlation with the local geometry of tetrahedral close-packing appears even in the correlation functions of the small models. In the quenched $CaAl_2$ phase, the peaks in $g_{Al\text{-}Al}(R)$ coincide very well with the first-, second, and third-nearest-neighbor Al-Al distances in the cubic Laves-phase $CaAl_2$, suggesting that the icosahedral arrangement around the Al sites exists in the quench-condensed as well as in the crystalline phase [see Fig. 5(a)]. In the Ca-rich glass-forming alloy Ca_7Al_3 we find that the peaks in $g_{Ca\text{-}Ca}(R)$ agree quite well with the near-neighbor Ca-Ca distances in the Laves phase, demonstrating that the local geometry is now dominated

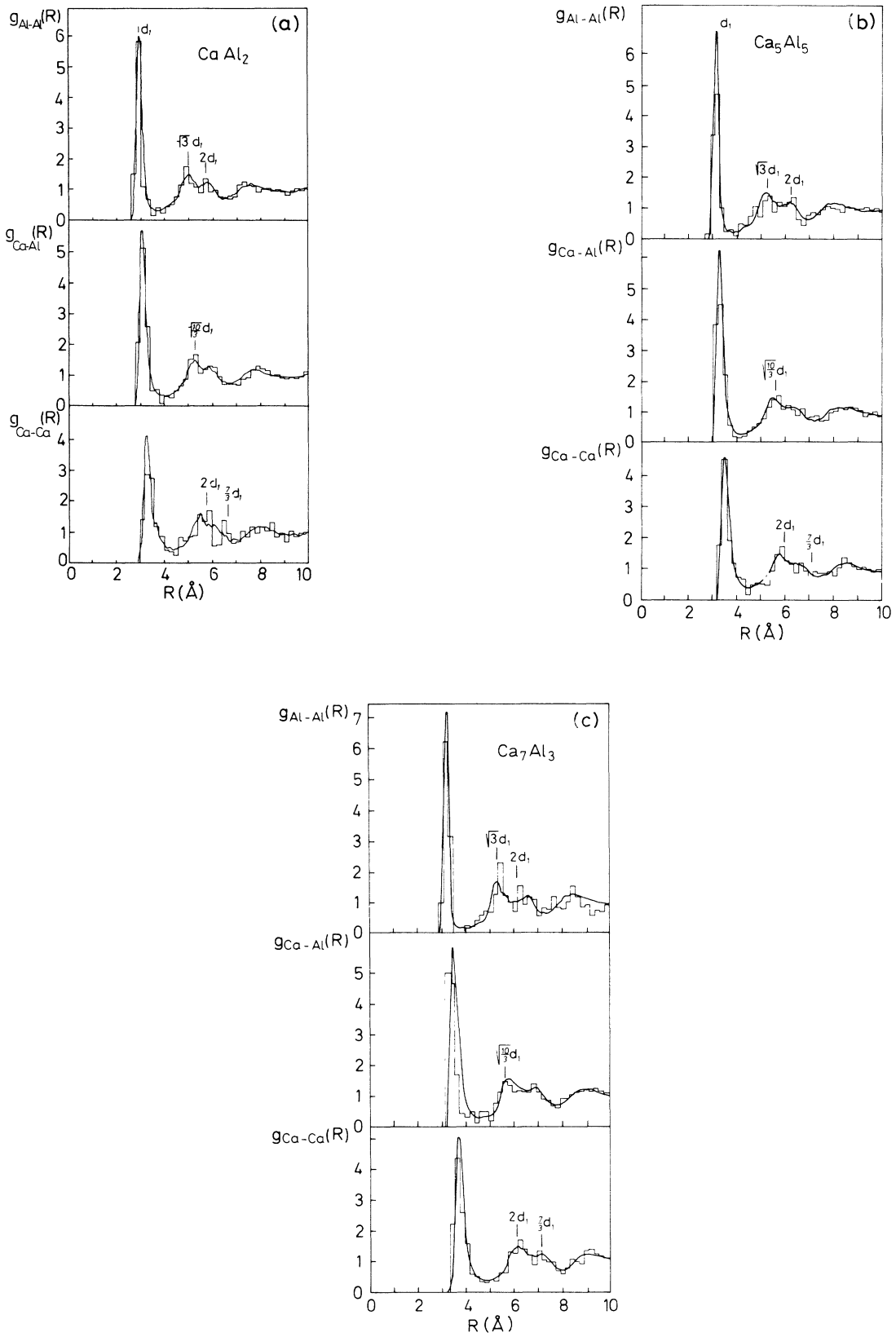

FIG. 5. Partial pair-correlation functions $g_{ij}(R)$ for amorphous Ca_xAl_{1-x} alloys [(a) $x=0.33$, (b) $x=0.50$, and (c) $x=0.70$]. The solid lines show the computer-simulation results obtained by the potential-energy mapping of 20 independent configurations of the 800-atom sample. The histogram represents the correlations functions of a single 60-atom model prepared out of one of these configurations (see text). The bars indicate the interatomic distances in a Laves-phase structure (d_1 is the shortest Al-Al distance).

by the Friauf-coordination polyhedra around the Ca sites with the icosahedra around the Al sites being considerably distorted [Fig. 5(c)]. At intermediate compositions the atomic structure shows a smooth transition between these two extremes [Fig. 5(b)].

IV. THE ELECTRONIC STRUCTURE OF AMORPHOUS AND CRYSTALLINE Ca-Al ALLOYS

A. Technical aspects

Our electronic-structure calculations have been performed using the linearized-muffin-tin-orbital (LMTO) method of Andersen *et al.*[30,31] Our reasons for adopting a supercell method and, in particular, the LMTO, have been given in paper I. Usually, supercell calculations are done for the Γ point [in fact, for $\mathbf{k}=(0.0, 0.0, 0.01)(\pi/a)$] of the Brillouin zone of the supercell only,[32,34] and a continuous DOS is derived from the discrete spectrum of the Γ-point energy eigenvalues by an appropriate Gaussian broadening (we use Gaussians with a width of 0.2 eV). As we had observed for the Ca-Mg glasses, we find for amorphous $CaAl_2$ that a calculation based on the Γ point only produces a DOS with a considerable structure (Fig. 6). If we extend the calculation to four Brillouin-zone points (we take the corners of the irreducible wedge), most of this structure disappears. The statistical representation of the electronic structure of the glass is further improved by taking the average over several different 60-atom models taken from independently mapped configurations (Fig. 6). As discussed in paper I, the combined Brillouin-zone– and configuration-averaging procedure gives reliable results for the electronic structure of simple-metal glasses. In the case of quench-condensed $CaAl_2$ the DOS is nearly parabolic and free-electron-like at higher binding energies ($E-E_F\sim-3$ eV), with a sudden onset of an increase at about 3 eV below the Fermi level.

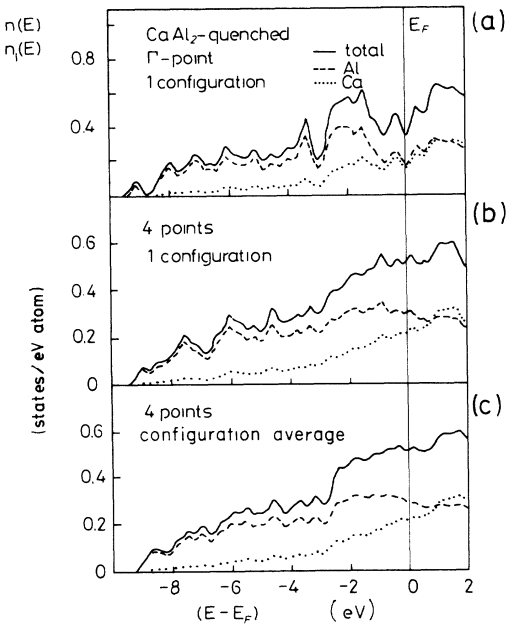

FIG. 6. Total and site-decomposed electronic densities of states (in states/eV atom) of amorphous $CaAl_2$ calculated for a 60-atom supercell using (a) only the Γ-point eigenvalues of a single model, (b) an average over the eigenvalues at four symmetry points, and (c) an average over four-point calculations of four different configurations (see text).

Brillouin and configuration averaging are not of the same importance at all compositions. In quenched $CaAl_2$ they are about equally important. In quenched Ca_7Al_3, on the other hand, we find only a slight difference between a Γ-point and a four-point calculation (Fig. 7), but again it is very important to take the configuration average. The necessity of taking a more extended Brillouin-zone average arises from the rather large dispersion of the free-electron-like bands.

B. The electronic structure of crystalline and amorphous $CaAl_2$

Figure 8 shows the band structure of the cubic ($MgCu_2$-type) Laves-phase $CaAl_2$, and the DOS calculated with the tetrahedron method[35] (using 89 points in the irreducible $\frac{1}{48}$ part of the Brillouin zone) is shown in Fig. 9(a). The band structure is quite similar to an earlier non-self-consistent pseudopotential calculation of Radwan and Taut.[36] Due to the much higher degeneracy than in fcc Al, the DOS is strongly structured with deep minima situated -7, -5, and -3 eV below the Fermi level and many sharp spikes just below and above the Fermi energy. The lowest three bands are occupied predominantly by Al $3s$ electrons, with an increasing admixture of Al $3p$ electrons with decreasing binding energy. The uppermost conduction band has Al $3p$ character, with a small admixture of Al $3s$ and Al $3d$ and Ca s,p,d states. Compared to fcc Al, the width of the occupied band is reduced from 11.6 eV (Ref. 37) to 9.0 eV, following the change of the free-electron value of the Fermi energy with decreasing electron density. The s,p hybridization is slightly reduced. The Ca states are spread out over a much larger energy range than in pure Ca and they show a strong s,p,d hybridization and a strong interaction with the Al states.

The calculated DOS can be compared with the x-ray-emission spectra of Wiech and Zöpf.[38] The $K\beta$-emission band of Al measures essentially the Al $3p$ DOS; the Al $L_{2,3}$-emission band measures the Al $3s$ and Al $3d$ DOS. In Fig. 10 we compare the measured x-ray spectra with the Gaussian-broadened partial densities of states (we use Gaussians with a half-width of 0.4 eV for the Al $3s$ and Al $3d$ DOS's, and with a half-width of 0.6 eV for the Al $3p$ DOS, corresponding to the different experimental resolution of the $L_{2,3}$ and $K\beta$ spectra[38]). The $L_{2,3}$ spectrum shows three characteristic peaks, confirming that the s and d electrons form relatively sharp subbands with little overlap. The position of these peaks correlates very well with the theoretical prediction. The main intensity of the $K\beta$ spectrum is concentrated in a rather narrow energy range (the width at half maximum being about

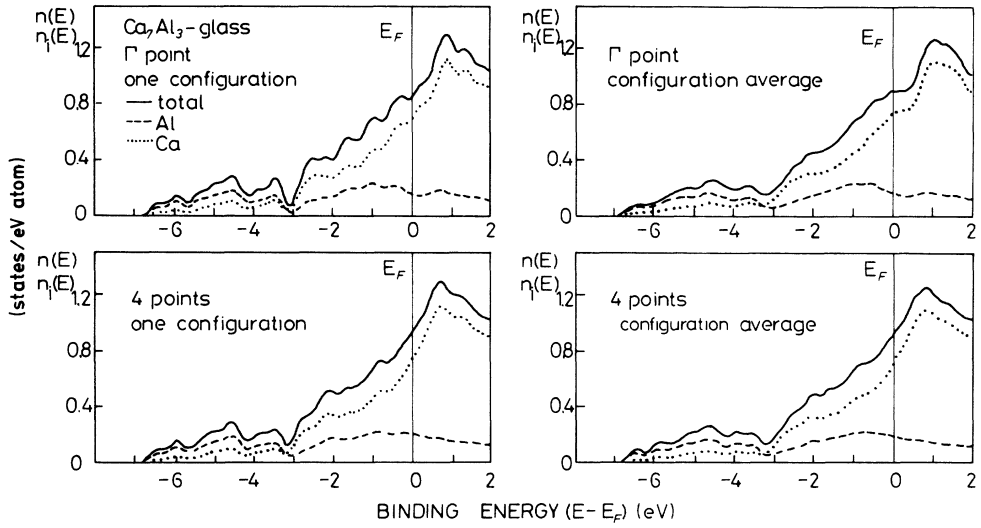

FIG. 7. Total and site-decomposed electronic densities of states (in state/eV atom) for amorphous Ca_7Al_3, comparing the effect of Brillouin-zone and configuration averaging (see Fig. 6 and text).

half that in pure Al), with weak structures at higher binding energies. Again we find good agreement between the measured x-ray-emission spectrum and the calculated DOS.

Next, we turn to the hypothetical amorphous $CaAl_2$ obtained by quench condensation of the liquid alloy. The calculated DOS [see Fig. 9(b)] shows that the sharp details related to the crystal structure disappear, but that the characteristic features of the electronic structures are preserved in the amorphous state: the width of the occupied conduction band is now 9.2 eV; the band separates rather distinctly into an Al $3s$-dominated part between -9 and -3 eV and an Al $3p$-dominated part (with a strong Ca s,p,d contribution) between -3 eV and the Fermi energy. At higher binding energies the DOS of the amorphous alloy is rather free-electron-like; from -3 eV onwards the DOS is enhanced over the free-electron value due to the admixture of Ca d states [$n(E_F)=0.43$ states/eV atom in the Laves phase and $n(E_F)=0.51$ states/eV atom in the amorphous phase, compared to a free-electron value of $n(E_F)=0.39$ states/eV atom].

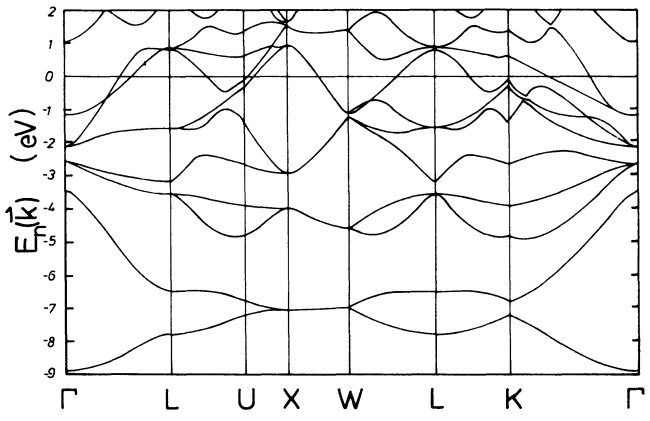

FIG. 8. The electronic band structure of the cubic Laves-phase $CaAl_2$.

C. The electronic structure of Ca-Al glasses

The electronic density of states of the metallic glasses Ca_xAl_{1-x} with $x=0.70$ to $x=0.50$ shows even larger deviations from a free-electron behavior (Figs. 11–13). The calculated bandwidth is now larger than that of the free-electron band. The DOS is lower than the free-electron values at higher binding energies, but strongly enhanced at the Fermi level (see Table I). The calculated $n(E_F)$ compares very well with electronic specific-heat data.[2] For all concentrations we find a minimum in the DOS at about -3 eV below the Fermi energy. The partial DOS's show that the lower part of the band is occupied almost exclusively by Al $3s$ electrons, with only a very small admixture of Al $3p$ and Ca electrons. The uppermost part of the occupied states consists of Al $3p$ orbitals which interact very strongly with the Ca s,p,d electrons. The integrated partial valence charges are compiled in Table II. The interatomic charge transfer is found to be small. More significant is the intra-atomic charge redistribution compared to the pure metals. We see that upon alloying with Al the Ca s charge is reduced, while the occupation of the d states is increased. On the Al sites, on the other hand, the s occupation is increased at the expense of the number of Al d electrons.

Thus we find that the electronic structure of the Ca-Al glasses is characterized by the complete dehybridization of the Al s,p band, and intra-atomic (s-d) and (d-s) promotions on the Ca and Al sites, respectively.

Again, it is interesting to make a comparison with the electronic structure of a crystalline intermetallic com-

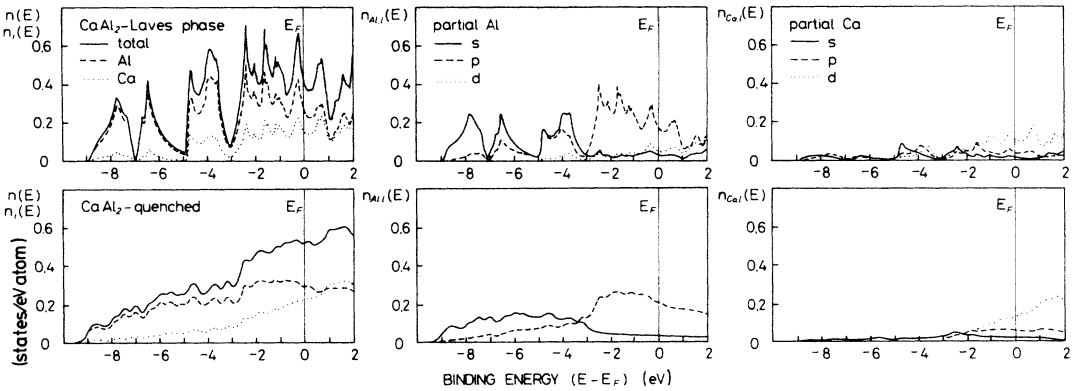

FIG. 9. Total, site-, and angular-momentum-decomposed electronic densities of states (in states/eV atom) for crystalline and amorphous $CaAl_2$.

pound of a similar composition. The phase diagram of the Ca-Al system[39] shows that there are no stable intermetallic compounds in the Ca-rich composition range (the only stable intermetallic compounds are the Laves-phase $CaAl_2$ and an incongruently melting $CaAl_4$ phase). Hence a possible crystal structure can only be guessed. Nagel *et al.*[9] have presented an augmented-spherical-wave (ASW) calculation for a hypothetical Ca_3Al compound with a cubic Cu_3Au structure, and Naugle *et al.*[7] have presented ASW results for a CaAl compound with the CsCl structure. It has often been suggested[7,9] that these calculations should be a valuable guide to the electronic structure of the amorphous alloys. We compare the Ca_3Al (Cu_3Au) DOS with our results for a-Ca_7Al_3 (Fig. 11). There are similarities as well as marked differences. We find the same splitting of the Al s and p states; the minimum in the DOS of the amorphous alloy becomes even a true gap in the crystalline compound. The partial valence charges are rather similar as well. On the other hand, the DOS of the crystalline compound shows strong structure close to the Fermi level which is completely absent in the amorphous alloy. Thus, the electronic-structure calculations for crystalline reference compounds could possibly serve to understand the main electronic bonding effects (and other properties related to the integrated density of states), but certainly cannot be used to interpret properties related to the differential density of states such as stability and optical or electronic transport properties.

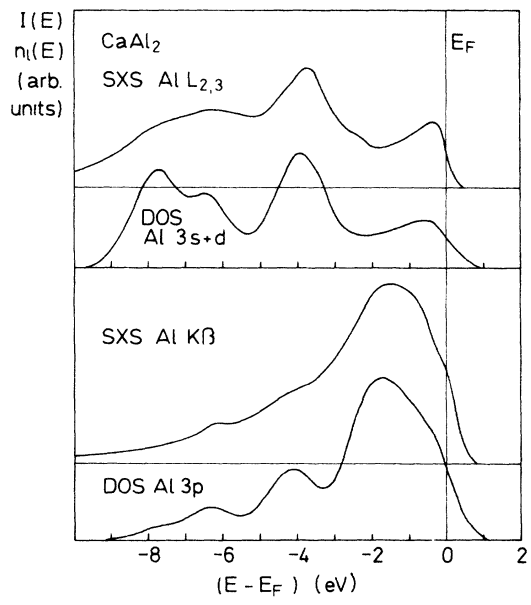

FIG. 10. Comparison of the Gaussian-broadened partial densities of state for the Laves-phase $CaAl_2$ with the soft-x-ray–emission spectra of Wiech and Zöpf (see text).

What is the physical mechanism behind these characteristic trends in the electronic DOS? The first and rather trivial point is that upon forming an A-B alloy, the A-A and B-B overlap will be reduced, hence the A and B subbands will be narrower than in the pure metals. In Ca-Al this effect is strong enough to split the free-electron s,p-conduction band of pure Al into neatly separate s and p parts in the Ca-Al glasses. The Al 3s band also does not hybridize with the Ca s states because of the large difference between the atomic Al 3s and Ca 4s levels ($E_{3s}^{Al}-E_{4s}^{Ca}=5.4$ eV). In Ca-Mg the closeness of the Mg 3s and Ca 4s levels leads to an appreciable interaction and hence to a much weaker structure in the DOS. The second point is the variation of the interatomic distances with concentration. We have found that the Al-Al distances change only little with the addition of Ca. If they change at all, they increase slightly. This would tend to enhance the dehybridization effect. The Ca—Ca bonds, on the other hand, are strongly contracted—this leads to a stronger Ca-Ca overlap, which even overcompensates for the reduction of the number of Ca-Ca neighbors and accounts for the increased s,p,d mixing on the Ca sites. These effects in the electronic structure are also strongly related to the chem-

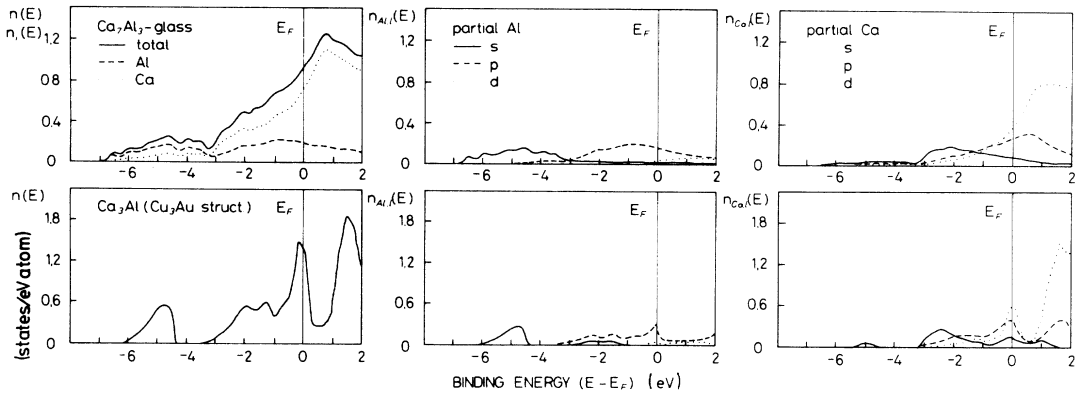

FIG. 11. Total, site-, and angular-momentum-decomposed electronic densities of states (in states/eV atom) for the metallic glass Ca_7Al_3 and for a crystalline Ca_3Al compound with a Cu_3Au structure (the results for Ca_3Al are taken from Nagel *et al.*, Ref. 9).

ical short-range order. This is most evident if we compare the DOS of a-Ca_7Al_3 (which has a more or less random distribution of the two atomic species; each Al atom has about four Al nearest neighbors) with that of x-Ca_3Al. In the Cu_3Au structure each Al atom in Ca_3Al has only Ca nearest neighbors. This is the reason for the even narrower Al $3s$ band in the crystalline compound and the formation of the gap at -4 eV.

Again, it is interesting to compare with experimental data. We have already shown that the rather high DOS at the Fermi level is in good agreement with the electronic specific-heat data. Figure 14 compares the calculated DOS with the photoemission data of Nagel *et al.*[9]—we find that the overall shape as well as details of the spectra such as the minimum at -3 eV and the broad maximum close to -5 eV are in good agreement with the ultraviolet-photoemission-spectroscopy (UPS) data. The partial Al $3p$ DOS compares very well with the Al $K\beta$ x-ray-emission spectrum (Fig. 15), confirming the predicted narrowing of the Al $3p$ band upon alloying.

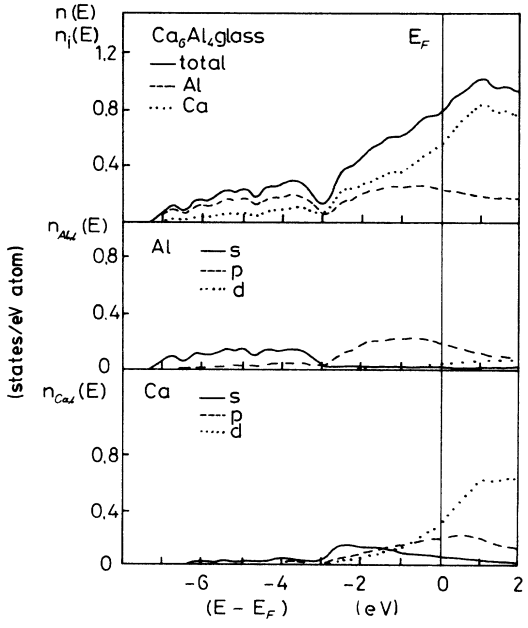

FIG. 12. Total, site-, and angular-momentum-decomposed electronic densities of states (in states/eV atom) for amorphous Ca_6Al_4.

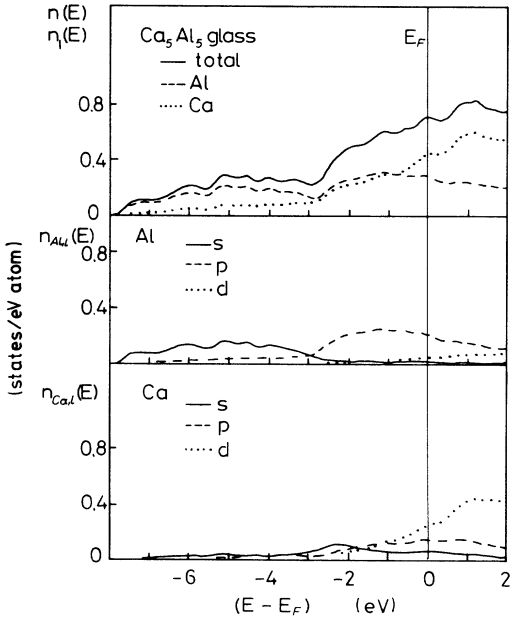

FIG. 13. Total, site-, and angular-momentum-decomposed electronic densities of states (in states/eV atom) for amorphous Ca_5Al_5.

TABLE I. Mean atomic volume V (in Å^3), width of the occupied band, W (in eV), and density of states at the Fermi level, $n(E_F)$ (in states/eV atom) in amorphous (a) and crystalline (x) Ca_xAl_{1-x} alloys.

		W		$n(E_F)$		
x	V	Calc.	FE[a]	Calc.	Expt.[b]	FE[a]
0.70 (a)	34.51	6.8	6.0	0.92	0.77	0.58
0.60 (a)	31.41	7.2	6.6	0.80	0.71	0.55
0.50 (a)	27.27	7.9	7.4	0.71		0.51
0.33 (a)	21.65	9.2	9.0	0.51		0.44
0.33 (x)	21.65	9.0	9.0	0.43		0.44

[a]Free-electron values.
[b]Heat-capacity measurements, Ref. 2.

V. CONCLUSIONS

We have presented an *ab initio* calculation of the atomic and electronic structure of Ca_xAl_{1-x} metallic glasses. The atomic structure is characterized by a large contraction of the Ca-Ca distances, which is attributed to an internal s-d-electron transfer on the Ca sites. The predicted contraction is well confirmed by diffraction data, which, however, show broader and more asymmetric peaks in the pair-correlation function than predicted by the computer simulation. We argue that this could be due to the extremely short electronic mean free path in these high-resistivity alloys leading to a damping of the oscillations in the effective interatomic interactions. The analysis of the local geometry shows that the local topology is that of a disordered tetrahedral close packing and points to substantial differences in the surroundings of Ca and Al atoms. In agreement with the local topology of the stable intermetallic compound, in the metallic glasses the Al atoms occupy sites with a predominantly icosahedral symmetry, whereas the coordination of the Ca atoms is very similar to the 14-, 15-, and 16-fold-coordinated Friauf polyhedra.

The electronic structure of the crystalline Laves-phase $CaAl_2$ is characterized by sharp structures in the DOS arising from the high degree of degeneracy. These structures are well confirmed by x-ray-emission experiments. In the amorphous $CaAl_2$ phase, these structure-induced features disappear and the resulting DOS is quite free-electron-like, except for an enhancement close to the Fermi level arising from the incipient occupation of the Ca $3d$ states.

The electronic DOS's of the metallic glasses Ca_xAl_{1-x} with $x=0.70$ to $x=0.50$ show rather pronounced deviations from a free-electron behavior. The strong s,p hybridization of the free-electron-like conduction band of pure Al is broken up. We find a relatively narrow Al $3s$ band between about -7 and -3 eV, and an Al $3p$ band at lower binding energies. Only the Al $3p$ band interacts with the Ca s,p,d states. Compared to the pure metals we find an intra-atomic s-d-electron transfer on the Ca sites (which accounts for the observed compression of the Ca—Ca bonds), and a d-s transfer on the Al sites. The DOS at the Fermi level is higher than the free-electron values, but the enhancement is smaller than in Ca-Mg glasses. There is no indication whatsoever for the often-postulated structure-induced DOS minimum at E_F. The calculated DOS is well confirmed by heat-capacity, photoemission, and soft-x-ray-emission experiments.

In tight-binding language the observed narrowing of the Al $3s$ and Al $3p$ subbands may be traced back to the reduction of the Al-Al overlap upon alloying with Ca. The weak interaction of the Al $3s$ band with the Ca conduction-band states arises from the large difference in the Al $3s$ and Ca $4s$ energy eigenvalues. At this point the Ca-Al system differs from the Ca-Mg alloys where the closeness of the Mg $3s$ and Ca $4s$ levels leads to a considerable Ca-Mg interaction over the entire width of the conduction band. The overlap argument makes it clear that the width of the subbands is related to the degree of chemical short-range order: a more pronounced ordering would lead to an even smaller subband width.[40]

In order to understand the relation between the effects observed in the electronic structure on one hand and the

TABLE II. Integrated partial valence-electron charges in amorphous Ca-Al alloys and in pure Ca and Al.

Ca_xAl_{1-x}	Z_l^{Ca}			Z_l^{Al}		
x	s	p	d	s	p	d
0.0				1.14	1.48	0.38
0.33	0.58	0.75	0.75	1.19	1.50	0.27
0.50	0.63	0.73	0.71	1.27	1.49	0.21
0.60	0.71	0.69	0.62	1.28	1.52	0.15
0.70	0.71	0.71	0.58	1.32	1.55	0.13
1.0	0.81	0.66	0.52			

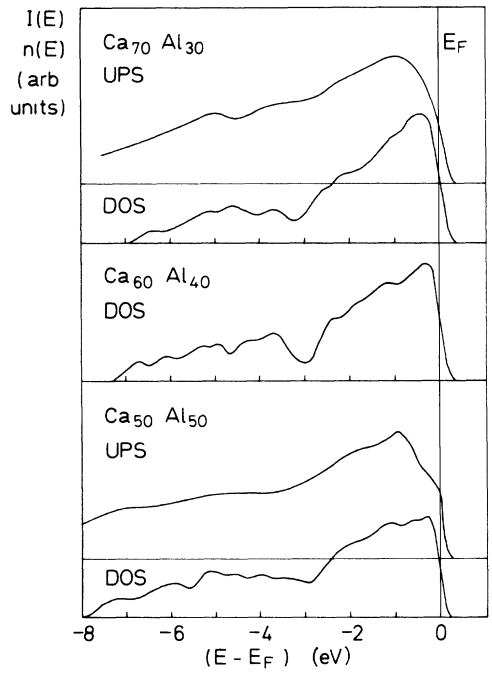

FIG. 14. Photoemission spectra for Ca-Al metallic glasses (Ref. 9) compared with the calculated electronic DOS.

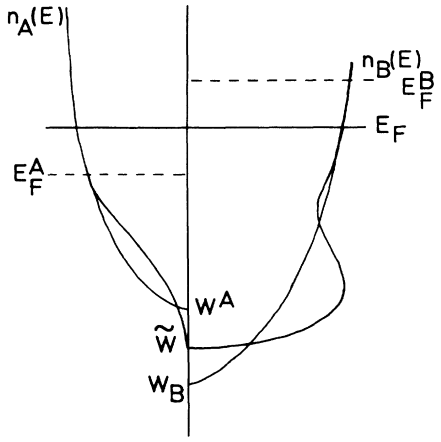

FIG. 16. Schematic illustration of the changes in the local DOS of two metals upon alloying (after Schlüter and Varma, Ref. 41). In the pure metals the bottom of the free-electron-like bands lies at the mean value of the pseudopotential W_i ($i=A,B$). After alloying the bottom of the common band is at the mean pseudopotential $\tilde{W}$. Near $\tilde{W}$ the local DOS is increased for the metal with the more attractive pseudopotential and rather low for the other one (see text).

concentration-dependent variation in the effective atomic interactions (and hence in the atomic structure) on the other, we follow a simple argument put forth by Schlüter and Varma.[41] In a pure simple metal, the lowest conduction-band eigenvalue will be determined by the mean pseudopotential W_i within the atomic cell. The essentially parabolic band will be filled up to the Fermi energy. In the alloy one will expect the following changes relative to the pure metals: The lowest state will lie at the self-consistent mean pseudopotential $\tilde{W}=(V_A W_A+V_B W_B)/(V_A+V_B)$ of the alloy (W_i and

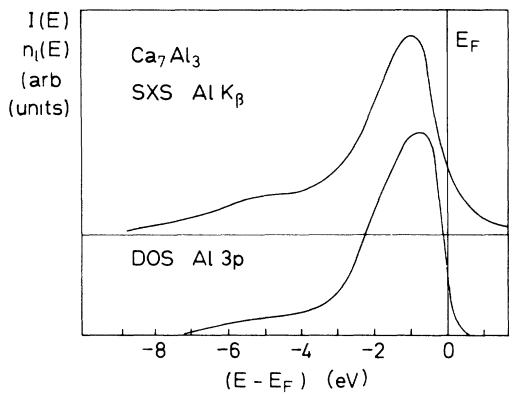

FIG. 15. The Al $K\beta$ x-ray–emission spectrum of the metallic glass Ca_7Al_3 (Ref. 9), compared with the partial Al $3p$ density of states.

V_i stand for the pseudopotential and the atomic volume of the species i in the alloy). Then if B is the component with the more attractive pseudopotential ($W_B<W_A$, here $B=$Al), states near the bottom of the conduction band will have large amplitudes in the B cells and small amplitudes in the A cells, i.e., $n_B(E)\gg n_A(E)$ for $E\sim\tilde{W}$, but for large kinetic energies both partial DOS's will converge to their free-electron values (except for a possible onset of d states). The situation is sketched schematically in Fig. 16. In a more complete treatment we have to allow for a nonlocality (i.e., an angular-momentum dependence) and a concentration dependence of the pseudopotentials W_i. As discussed at the end of Sec. II, a weaker orthogonalization effect results in a stronger electron-ion pseudopotential, and this will affect the s component of the conduction-band states more than their p and d components. This is just what the electronic-structure calculations give for the partial Al DOS: stronger s bonding and weaker p and d bonding. Conversely, the stronger orthogonalization effect leads to a strengthening of the d-electron bonding on the Ca sites and a weaker s-electron bonding. Thus, pseudopotential perturbation theory and LMTO calculations offer a consistent picture.

The present electronic-structure calculations are in qualitative agreement with the electronic transport data. Mizutani *et al.*[8] have pointed out that the Hall-effect data yield an effective electron concentration (e/A) close to the nominal one in Ca-Mg glasses, but substantially lower in ternary Ca-Mg-Al and Ca-Al glasses. If we assume that the electrons in the nearly separate low-lying Al $3s$ band do not contribute to the electronic transport,

we find $e/A = 1.9$ for a-Ca_7Al_3 compared to a nominal value of $e/A = 2.3$. Mizutani *et al.* also point to a relation between an increasing electrical resistivity and a decreasing $n(E_F)$ given by our calculations. Further details must be left to an actual calculation of the electronic transport properties for which our present work provides a useful basis. Finally, a *self-consistent* calculation of the electronic *and* the atomic structure is necessary to resolve the remaining difficulties with the atomic structure of Ca-Al glasses.

ACKNOWLEDGMENTS

One of us (S.S.J.) acknowledges support from the Fulbright Foundation.

*On leave of absence from Behlen Laboratory of Physics, University of Nebraska, Lincoln, NE 68588.

[1]J. Hafner and A. Phillip, J. Phys. F **14**, 1685 (1984).
[2]U. Mizutani, Prog. Mater. Sci. **28**, 97 (1983).
[3]U. Mizutani and T. Matsuda, in *Proceedings of the 5th International Conference on Rapidly Quenched Metals,* edited by S. Steeb and H. Warlimont (North-Holland, Amsterdam, 1985), Vol. 1, p. 1035.
[4]D. P. Love, F. C. Wang, D. G. Naugle, C. L. Tsai, B. C. Giessen, and T. O. Callaway, Phys. Lett. **90A**, 303 (1982).
[5]U. Mizutani and T. Matsuda, J. Phys. F **13**, 2115 (1983).
[6]J. Erwin, R. Delgado, H. Armbruster, D. G. Naugle, D. P. Love, F. C. Wang, C. L. Tsai, and T. O. Callaway, Phys. Lett. **100A**, 97 (1984).
[7]D. G. Naugle, R. Delgado, H. Armbruster, C. L. Tsai, T. O. Callaway, D. Reynolds, and V. L. Moruzzi, Phys. Rev. B **34**, 8279 (1986).
[8]U. Mizutani, M. Sasaura, Y. Yamada, and T. Matsuda, J. Phys. F **17**, 667 (1987).
[9]S. R. Nagel, U. Gubler, C. F. Hague, J. Krieg, R. Lapka, P. Oelhafen, H. J. Güntherodt, J. Evers, A. Weiss, V. L. Moruzzi, and A. R. Williams, Phys. Rev. Lett. **49**, 57 (1982).
[10]E. Nassif, P. Lamparter, and S. Steeb, Z. Naturforsch. **38a**, 1206 (1983).
[11]J. Hafner, T. Egami, S. Aur, and B. C. Giessen, J. Phys. F **17**, 1807 (1987).
[12]J. Hafner and S. S. Jaswal, J. Phys. F **18**, L1 (1988).
[13]S. S. Jaswal and J. Hafner, the preceeding paper, Phys. Rev. B **38**, 7311 (1988).
[14]W. B. Pearson, *The Crystal Physics and Chemistry of Metals and Alloys* (Wiley-Interscience, New York, 1972).
[15]J. Hafner, Phys. Rev. B **21**, 406 (1980).
[16]J. Hafner, in *From Hamiltonians to Phase Diagrams—The Electronic and Statistical-Mechanical Theory of sp-Bonded Metals and Alloys,* Vol. 70 of *Springer Series in Solid State Sciences,* edited by P. Fulde, M. Cardona, H. Queisser, and K. von Klitzing (Springer, Berlin, 1987).
[17]J. Hafner, J. Phys. F **15**, 1879 (1985).
[18]W. Geertsma, J. Dijkstra, and W. van der Lugt, J. Phys. F **14**, 1833 (1984).
[19]F. Springelkamp, R. A. de Groot, W. Geertsma, W. van der Lugt, and F. M. Mueller, Phys. Rev. B **32**, 2319 (1985).
[20]L. Pauling, *The Nature of the Chemical Bond* (Cornell University Press, Ithaca, 1952), Chap. 12.6.
[21]R. Evans, in *Electrons in Disordered Metals and at Metallic Surfaces,* Vol. 42, Series B of the NATO Advanced Study Institute, edited by P. Phariseau, B. L. Györffy, and L. Scheire (Plenum, New York, 1979), p. 417.
[22]J. Hafner and V. Heine, J. Phys. F **13**, 2479 (1983); **16**, 1429 (1986).
[23]F. H. Stillinger and T. A. Weber, J. Chem. Phys. **80**, 4434 (1984); Phys. Rev. B **31**, 5262 (1985).
[24]T. A. Weber and F. H. Stillinger, Phys. Rev. B **31**, 1954 (1985).
[25]J. Hafner, in Proceedings of the 6th International Conference on Liquid and Amorphous Metals, edited by E. Lüscher, W. Gläser, and F. Hensel [Z. Phys. Chem. **157**, 115 (1988)].
[26]J. Hafner, J. Phys. F **18**, 133 (1988).
[27]J. Hafner, J. Phys. (Paris) Colloq. **46**, C9-62 (1985).
[28]D. R. Nelson, Phys. Rev. Lett. **50**, 982 (1983).
[29]D. R. Nelson and S. Sachdev, in *Amorphous Metals and Semiconductors,* edited by P. Haasen and R. I. Jaffee, Acta-Scripta Metallurigca Proc. Ser. No. 3 (Pergamon, Oxford, 1986), p. 28.
[30]O. K. Andersen, O. Jepsen, and D. Glötzel, in *Highlights of Condensed Matter Theory,* edited by F. Bassani, F. Fumi, and M. P. Tosi (North-Holland, Amsterdam, 1985).
[31]H. L. Skriver, in *The LMTO Method,* Vol 41 of *Springer Series in Solid State Sciences,* edited by P. Fulde, M. Cardona, and K. von Klitzing (Springer, Berlin, 1981).
[32]S. S. Jaswal and W. Y. Ching, Phys. Rev. B **26**, 1064 (1982).
[33]S. S. Jaswal, Phys. Rev. B **34**, 8937 (1986).
[34]S. S. Jaswal, D. J. Sellmyer, M. Engelhardt, Z. Zhao, A. J. Arko, and K. Xie, Phys. Rev. B **35**, 996 (1987).
[35]O. Jepsen and O. K. Andersen, Solid State Commun. **9**, 1762 (1971); G. Lehmann and M. Taut, Phys. Status Solidi B **54**, 469 (1972).
[36]A. M. Radwan and M. Taut, Phys. Status Solidi B **76**, 605 (1976).
[37]V. L. Moruzzi, J. F. Janak, and A. R. Williams, *Calculated Electronic Properties of Metals* (Pergamon, New York, 1978).
[38]G. Wiech and E. Zöpf, in *Band Structure Spectroscopy of Metals and Alloys,* edited by D. J. Fabian and L. M. Watson (Academic, London, 1973), p. 173.
[39]M. Hansen and K. Anderko, *The Constitution of Binary Alloys,* 2nd ed. (McGraw-Hill, New York, 1958).
[40]A. Pasturel and J. Hafner, Phys. Rev. B **32**, 8357 (1986).
[41]M. Schlüter and C. M. Varma, Phys. Rev. B **23**, 1633 (1981).